

A coupled ecohydrodynamic model to predict algal blooms in Lake Titicaca

François Duquesne^a, Valentin Vallaëys^a, Prem Jai Vidaurre^b, Emmanuel Hanert^{a,c,*}

^a UCLouvain, Earth and Life Institute (ELI), Louvain-la-Neuve, Belgium

^b Universidad Mayor de San Andrés, Instituto de Ecología (IE), La Paz, Bolivia

^c UCLouvain, Institute of Mechanics, Materials and Civil Engineering (IMMC), Louvain-la-Neuve, Belgium

ARTICLE INFO

Keywords:

Lake Titicaca
Hydrodynamic model
NPZD ecosystem model
Algal bloom
Water quality
SLIM

ABSTRACT

Lake Titicaca is home to a unique high-altitude ecosystem that is suffering from increasing anthropogenic pressures. It experienced its first major algal bloom in March–April 2015 that had devastating consequences in the southern shallow lake basin. Such events are expected to intensify in the future and call for a more active and quantitative management of the lake and its watershed. In this paper we describe a coupled ecohydrodynamic model to predict the lake's water quality and, more particularly, the risk of harmful algal blooms. We have coupled a nitrogen-phytoplankton-zooplankton-detritus (NPZD) ecosystem model to the unstructured-mesh 3D hydrodynamic model SLIM. Our high-resolution multi-scale model explicitly represents the exchanges between the two basins composing the lake, through the narrow Strait of Tiquina. This allowed us to study the biophysical processes driving the entire lake over the period of January 2014 to May 2015. The model has been validated against temperature profiles at several locations throughout the lake. It correctly reproduces the seasonal temperature variations that drive the lake stratification and impact the vertical distributions of phytoplankton. Our model was able to replicate the space–time dynamics of the March–April 2015 algal bloom similarly to what was observed on satellite imagery. We believe that our multi-scale ecohydrodynamic model is a promising tool to complement field observations and hence support water management in the lake and its watershed.

1. Introduction

With a surface area of 8372 km², Lake Titicaca is the largest freshwater lake in South America and, sitting at 3812 m altitude, is the highest of the world's large lakes. It is nested within the Altiplano, a high plateau region shared by Peru and Bolivia in the Andes mountain range. Lake Titicaca is part of the larger Titicaca-Desaguadero-Poopó-Salar de Coipasa (TDPS) watershed system, which spans mostly over Bolivia and Peru, and encompasses parts of northern Chile. The high plateau is one of the poorest areas of Peru and Bolivia, with 73.5% of the population having at least one basic need that was not met in 2001 (Martine Gonzales et al., 2007). Lake Titicaca is thus one of the most important natural resources in the region. Historically, it has been essential for the development of important Andean cultures such as the Tiwanaku and still provides food and raw materials to the Aymara communities. The lake is also a strong driver for tourism, attracting millions of tourists every year. Unfortunately, it is also subject to the inevitable impact of human activities on its ecosystem. In order to ensure the welfare of the lake, the countries of Peru and Bolivia have reached agreements on the joint management of hydrological and

hydrobiological resources of the lake and its basin. The Autonomous Binational Authority of the Lake Titicaca Water System (ALT) was created for this purpose in 1996 insuring the responsible water management of the entire TDPS system. This has led to several research and sanitation projects on the Bolivian side by the Ministry of Environment and Water.

Lake Titicaca water quality has been a subject of concern in recent years. Over the past decade, mining activities in the region have been pointed out as the cause for mercury and heavy metal contamination (Gammons et al., 2006; Monroy et al., 2014; Guedron et al., 2017; Molina et al., 2017). Human activities in general have been related to water quality degradation through metal and bacterial contamination (Ap et al., 2017), antibiotics contamination (Duwig et al., 2014; Archundia et al., 2017), and contamination by trace elements such as arsenic (Lima et al., 2019; Sarret et al., 2019). The increasing populations of the numerous cities around the lake indicate that the contamination is likely to intensify in the years to come. All of these pollutions have a negative impact on the aquatic biota and on the lake ecosystem as a whole. Numerous species are affected and, if no actions are taken, some native species such as the emblematic frog *Telmatobius culeus* could become extinct.

* Correspondence to: UCLouvain/ELI/ELIE, Croix du Sud 2 box L7.05.16, B-1348 Louvain-la-Neuve, Belgium.
E-mail address: emmanuel.hanert@uclouvain.be (E. Hanert).

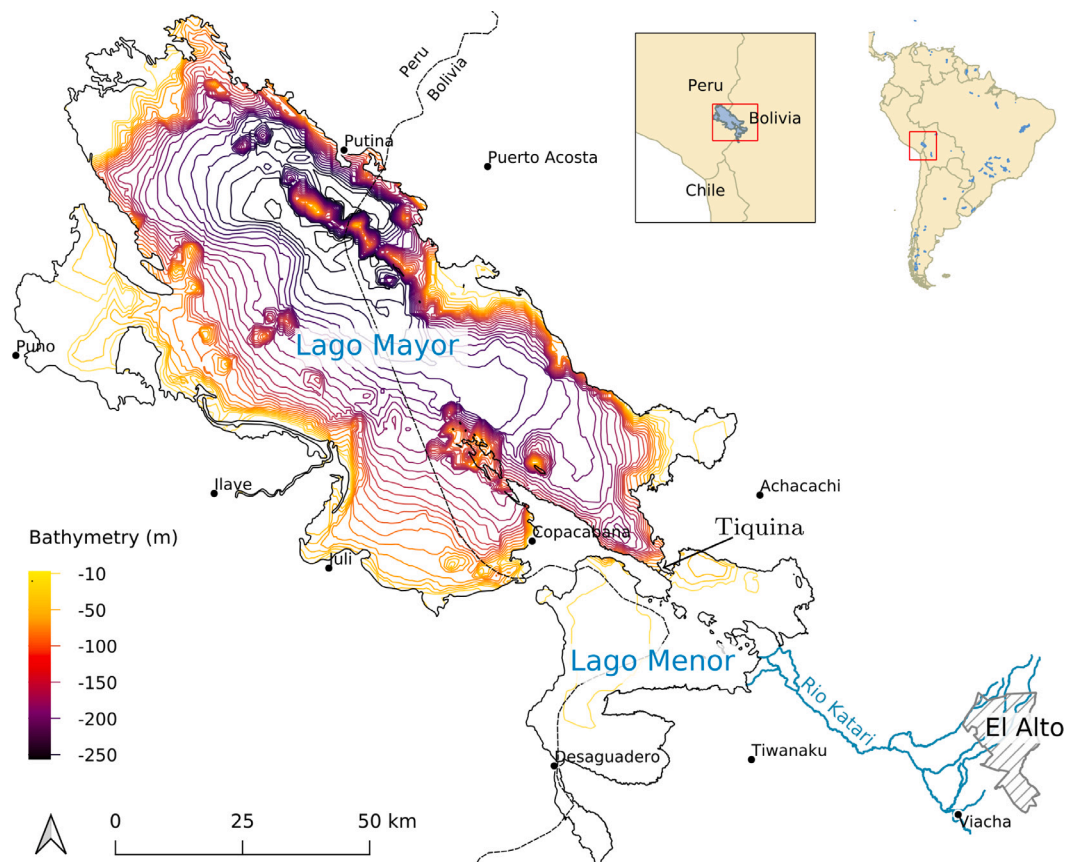


Fig. 1. Overview of Lake Titicaca with its two basins, Lago Mayor in the North and Lago Menor in the South, connected by the narrow Strait of Tiquina. Depth contour lines are 10 m apart. The Katari River (Rio Katari) is the main inflow of Lago Menor.

The increasing frequency of pollution calls for an active management of the lake and its watershed. However, this natural ecosystem being large and complex, it requires a sophisticated measurement system in order to efficiently manage water quality. In this context, mathematical models can be greatly beneficial since they can take into account the complexity of the ecosystem through a set of equations and can simulate its behavior under different conditions. Given the correct inputs, a good model efficiently represents the biophysical state of the lake, accomplishing the task of monitoring water quality with significantly less resources. Furthermore, models allow us to simulate the effects of different scenarios regarding pollution and remediation. This provides valuable insights when it comes to choosing appropriate solutions for investing in water quality improvements. They can also help us to anticipate the impact of future anthropogenic contamination and therefore take actions in order to limit the environmental impact.

Several models exist for this purpose and have been developed for different types of water bodies. The NPZD (for Nitrogen-based nutrients, Phytoplankton, Zooplankton, and Detritus) ecosystem model is one of the most widely-used (see for instance Olascoaga et al. (2005), Luo et al. (2012), Tian et al. (2015)). This is mainly due to the fact that it is relatively simple and does not require many parameters, yet it is capable of generating realistic results. Other variants of this type of model have also been introduced by refining some components. For instance, the nutrient component can be subdivided into NO_3 and NH_4 , or the phytoplankton can be seen as flagellates, cyanobacteria and diatoms. New components such as the dissolved oxygen or the silica content can also be integrated. However, the basic NPZD type model remains the first option for most water quality modeling works.

In this paper, we describe a coupled ecohydrodynamic model to study the nutrient-plankton dynamics in Lake Titicaca. The hydrodynamic component is covered with SLIM3D, the 3D version of the

multi-scale hydrodynamic model SLIM.¹ The ecosystem component is represented with a NPZD ecosystem model coupled to SLIM3D. Such a modeling approach has already been applied to many lakes, including Lake Zurich (Omlin et al., 2001), Lake Tanganyika (Naithani et al., 2007) and Lake Chini (Sharip et al., 2016), but, to our knowledge, this is the first application to Lake Titicaca. The goal set for our study is to simulate the annual evolution of the lake's biophysical state and reproduce the occurrence of an algal bloom event triggered by nutrients originating from the Katari River. A qualitative validation of our model is performed by comparing our results with observations and the satellite imagery during the bloom event.

2. Material and methods

In this section, we describe the geography and climatology of Lake Titicaca before deriving the eco-hydrodynamic model equations and summarizing the model forcings.

2.1. Study area

Lake Titicaca is composed of two main parts: Lago Mayor in the North (83.4% of the total surface and reaching depths of 250 m) and the smaller and shallower Lago Menor in the South (average depth of 9 m and max depth of 42 m) (Wirrmann et al., 1992) (see Fig. 1). These two parts are connected by the Strait of Tiquina, a short (about 3 km), narrow (mostly less than 1 km) passage, with a steep sloping bathymetry that goes from about 20 m in Lago Menor to 50 m in Lago

¹ SLIM: Second-generation Louvain-la-Neuve Ice-Ocean Model, www.slim-ocean.be.

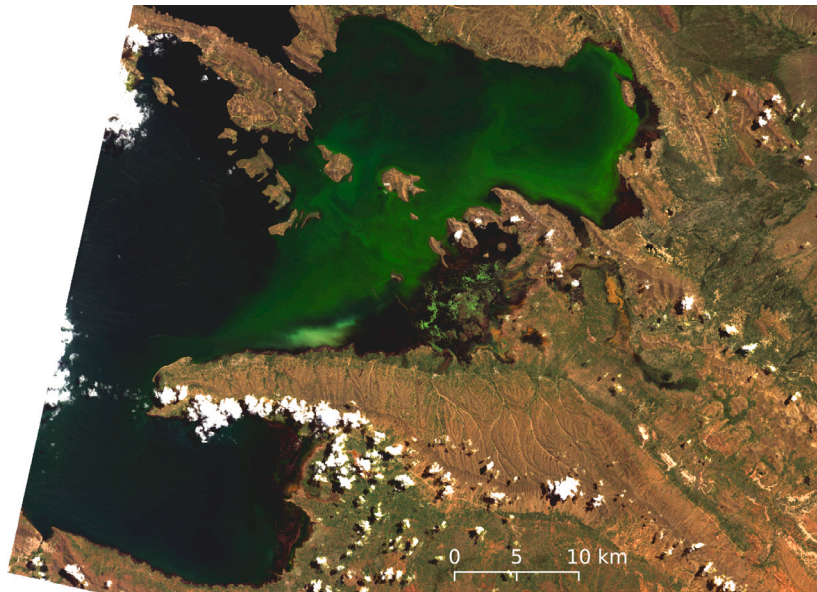


Fig. 2. Landsat 8 imagery of Lago Menor taken on the 24th of March 2015.

Mayor. The main water inputs to the lake are: rainwater (55%), inflow by rivers (44%) and groundwater inflows (1%). The main outputs are evaporation (95%) and outflow through the Desaguadero River (5%). Other losses are negligible (Martine Gonzales et al., 2007). The main forcings that affect the water dynamics within the lake are limited to the heat and momentum exchanges with the atmosphere. Since the lake is situated between the latitudes of -15.2°S and -16.6°S , its climate is conditioned by a dry season spanning from April to September and a warmer wet season during the rest of the year. The lake surface temperatures vary from an average of 16°C at the peak of the wet season to around 12°C in the midst of the dry season. Daily variations have an approximate mean amplitude of 4°C . Winds mainly blow towards the southwest descending from the Cordillera Real with a mean velocity of about 1.5 m/s .

The shallow regions of Lake Titicaca such as the Puno Bay and Lago Menor have been identified as the most contaminated and the most subject to algal blooming in the past years. In particular, the southeastern side of Lake Titicaca is often affected by pollution due to the important anthropogenic activities upstream. The Katari River, which flows into Lago Menor (Fig. 1), carries water that is contaminated by the highly populated city of El Alto (9.22×10^5 inhabitants in 2018 according to the Bolivian National Institute of Statistics) and by the municipalities of Viacha, Laja, Pucarani and Puerto Perez along the river banks (Duwig et al., 2014; Ap et al., 2017; Archundia et al., 2017). The uncontrolled urban wastewater discharges lead to high concentrations of nitrates and other nutrients that make their way to the lake, where they create eutrophic conditions. Hence, in this portion of the lake, algal bloom events have become seasonal. The particularly strong bloom event of March–April 2015 serves as a good example. Fig. 2 is a true color Landsat 8 image of Lago Menor taken on the 24th of March 2015. The algal bloom mainly covers the eastern part of the basin. More than half the surface of Lago Menor was affected and more than two tonnes of aquatic biota deaths were reported.

The main algae involved during the March–April 2015 bloom was *Carteria* sp. (Acha et al., 2018), which is a type of green algae having four flagella. Komarkova et al. (2016) have shown that algal blooms in Lake Titicaca can also involve cyanobacteria, as is often the case for blooms associated with high concentrations of nutrients in the water. They also provide a description of the species composition of phytoplankton assemblages in the lake. In addition to cyanobacteria, there are also dinoflagellates and green algae. Diatoms are not very common. A description of the zooplankton species present in the lake can be found in Widmer et al. (1975).

2.2. Hydrodynamic model

The spatial extent and concentration of algal blooms are directly influenced by the lake hydrodynamics. Here, we simulate it by means of SLIM3D, which solves the three-dimensional hydrostatic equations under the Boussinesq approximation on a 3D mesh made out of triangular prisms. Unlike traditional hydrodynamic models, SLIM uses an unstructured horizontal mesh that accurately represents the lake topography, including narrow passages such as Tiquina Strait. It solves the model equations with the Discontinuous Galerkin (DG) finite element method, which combines the accuracy of finite elements and the local conservation properties of finite volumes. SLIM3D has been previously applied to a number of different environments such as the Columbia River estuary (Vallaey et al., 2018), Lake Tanganyika (Delandmeter et al., 2018), the Burdekin River estuary (Delandmeter et al., 2015) or the Congo River estuary (Vallaey et al., 2020).

The model governing equations can be written as follows:

$$\frac{\partial \mathbf{u}}{\partial t} + \nabla_h \cdot (\mathbf{u}\mathbf{u}) + \frac{\partial(w\mathbf{u})}{\partial z} = \nabla_h \cdot (\nu_h \nabla_h \mathbf{u}) + \frac{\partial}{\partial z} \left(\nu \frac{\partial \mathbf{u}}{\partial z} \right) - f \mathbf{e}_z \wedge \mathbf{u} - g \nabla_h \eta \quad (1)$$

$$- \frac{g}{\rho_0} \nabla_h \int_z^\eta (\rho - \rho_0) dz - \frac{1}{\rho_0} \nabla_h p_a, \quad \nabla_h \cdot \mathbf{u} + \frac{\partial w}{\partial z} = 0, \quad (2)$$

$$\frac{\partial T}{\partial t} + \nabla_h \cdot (\mathbf{u}T) + \frac{\partial(wT)}{\partial z} = \nabla_h \cdot (\kappa_h \nabla_h T) + \frac{\partial}{\partial z} \left(\kappa \frac{\partial T}{\partial z} \right) + f_{\text{relax}}, \quad (3)$$

where the unknowns are the horizontal velocity $\mathbf{u} = (u, v)$, the vertical velocity w and the temperature T . An external mode solves the fast propagating waves to compute the free surface elevation η . The temperature impacts the water density ρ through the equation of state of Jackett et al. (2006). The horizontal viscosity ν_h follows the parametrization of Smagorinsky (1963) and the horizontal diffusivity κ_h the parametrization of Okubo (1971). A second-order turbulence closure provides the vertical viscosity ν and diffusivity κ . Other parameters are f , the Coriolis parameter, $\rho_0 = 1005\text{ kg/m}^3$, the constant reference density, and $g = 9.81\text{ m}^2/\text{s}$, the gravitational acceleration. The mathematical symbols \mathbf{e}_z , ∇_h and \wedge respectively stand for the vertical unit vector (pointing upward), the horizontal derivative operator and the vector product operator. For more information regarding these equations, see Vallaey et al. (2018).

In our study, Lake Titicaca is considered as an entirely closed system regarding the water mass balance and we assume equilibrium between

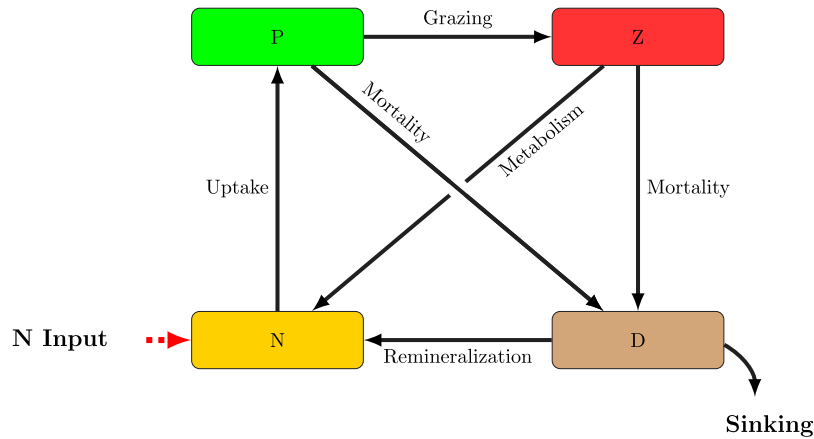


Fig. 3. Main processes involved in the evolution of the four components of the NPZD ecosystem model.

inputs and outputs of water. In order to parameterize the heat flux based on the difference between prescribed surface temperature and the computed temperature in the top layers of the lake, a temperature relaxation term f_{relax} is included in Eq. (3) :

$$f_{relax} = \frac{\max(z_r + z, 0)}{z_r \tau_r} (T_{surface} - T), \quad (4)$$

where the depth of the relaxation zone ($z_r = 25$ m) and the relaxation time ($\tau_r = 5$ days) have been calibrated empirically. This relaxation term linearly decays from a maximum value at the surface of the lake to zero when $z \leq -z_r$.

2.3. Ecosystem model

To assess the effect of land-based activities on the lake, we have developed an ecosystem model that is coupled with the hydrodynamic model. It simulates the space–time dynamics of four variables: Nitrogen-based nutrients (N), Phytoplankton (P), Zooplankton (Z) and Detritus (D). The biochemical processes linking these variables together are summarized in Fig. 3. Our model is based on the work of Tian et al. (2015) with some parameter values adapted to Lake Titicaca.

In a NPZD model, there is an uptake of nutrients by phytoplankton through photosynthesis. The growing phytoplankton is subject to mortality and to grazing by zooplankton. This zooplankton can redistribute nutrients through its metabolism (excretions) and is also subject to mortality. Finally, the detritus stock is replenished by the dead phytoplankton and zooplankton. Detritus provide nutrients through remineralization and are subject to sinking forces. In addition to these basic processes, an external input of nutrients is added in order to simulate the contribution of nutrient rich waters from the Katari River due to the upstream anthropogenic activities.

All the variables of the NPZD model are transported by the flow. It therefore runs simultaneously with the hydrodynamic model. The coupling between both models is only “one way” as the NPZD model requires the velocity and temperature fields computed by the hydrodynamic model but the latter is not influenced by the NPZD model outputs. The governing equations of the ecosystem model can be written as follows:

$$\frac{\partial N}{\partial t} + A(N) = -U_P + \lambda G_Z + \epsilon f_1(T)D + D(N), \quad (5)$$

$$\frac{\partial P}{\partial t} + A(P) = U_P - G_Z - m_p f_1(T)P^2 + D(P), \quad (6)$$

$$\frac{\partial Z}{\partial t} + A(Z) = \gamma G_Z - m_z f_1(T)Z^2 + D(Z), \quad (7)$$

$$\frac{\partial D}{\partial t} + A(D) = (1 - \gamma - \lambda)G_Z + m_p f_1(T)P^2 + m_z f_1(T)Z^2 - \epsilon f_1(T)D + \frac{\partial(s_D D)}{\partial z} + D(D), \quad (8)$$

where the advection (A) and diffusion (D) terms for a component X are defined as follows:

$$A(X) = \nabla_h \cdot (\mathbf{u}X) + \frac{\partial(wX)}{\partial z}, \quad (9)$$

$$D(X) = \nabla_h \cdot (\kappa_h \nabla_h X) + \frac{\partial}{\partial z} \left(\kappa \frac{\partial X}{\partial z} \right), \quad (10)$$

where \mathbf{u} and w are the horizontal and vertical velocities computed by the hydrodynamic model. The diffusivity coefficients κ_h and κ are assumed to be identical to those used in Eq. (3) for the temperature.

In Eq. (8), the vertical advection term with a velocity s_D represents the sinking of detritus to the bottom of the lake. A similar term could also be used in the phytoplankton equation to account for phytoplankton sinking. Here we chose not to consider it as we are mostly interested in developing a model that can predict the occurrence of algal blooms. In freshwater systems, algal blooms are often the result of a sudden increase in cyanobacteria. These photosynthetic bacteria tend to form gas vesicles that allow them to float at the surface. Cyanobacteria therefore remain in the upper illuminated water layer of a stratified lake and hence increase their total daily light dose, which further enhances their growth. In the particular case of the 2015 algal bloom in Lake Titicaca, which we consider in this paper, Acha et al. (2018) have shown that the algae involved in the bloom were almost entirely *Carteria* sp., which are not cyanobacteria but a type of green algae having four flagella. These algae have a small, albeit non-zero, sinking velocity of about 0.2 m/day (Bienfang and Harrison, 1984). In our NPZD model, we have therefore assumed that the phytoplankton compartment is only composed of bloom-forming algae for which the sinking velocity is small enough to be neglected. A more realistic model would of course distinguish between different phytoplankton species but this is beyond the scope of this paper.

The uptake (U_P) and grazing (G_Z) terms are defined as:

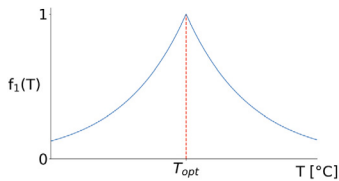
$$U_P = \mu_{max} f_1(T) f_2(N) f_3(I) P, \quad (11)$$

$$G_Z = g_{max} f_1(T) f_4(P) Z. \quad (12)$$

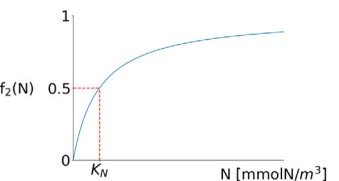
Nitrogen uptake is topped by a maximum growth rate for phytoplankton μ_{max} and is influenced by the temperature through $f_1(T)$, the availability of nitrogen through $f_2(N)$ and the phytoplankton response to light through $f_3(I)$. Grazing, on the other hand, is limited by the zooplankton maximum grazing rate g_{max} , by the amount of phytoplankton available for grazing through $f_4(P)$ and by temperature through $f_1(T)$.

The effect of temperature on grazing and nutrient uptake is parameterized as an exponential function decreasing from an optimal

temperature T_{opt} .

$$f_1(T) = e^{-a|T-T_{opt}|} \quad (13)$$


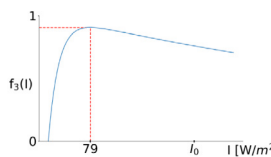
Nitrogen availability is parameterized by a Michaelis–Menten function characterized by the half-saturation constant for nitrogen uptake K_N .

$$f_2(N) = \frac{N}{N + K_N} \quad (14)$$


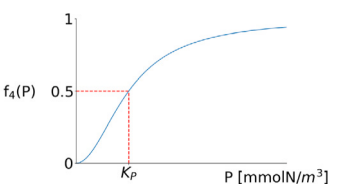
Solar radiation also plays an important role since it is the main driver of photosynthesis. Solar radiation reaches the lake surface with a surface photosynthetically active radiation (PAR) of 275 W/m^2 . This value is particularly large since Lake Titicaca is situated in high altitude where solar radiation is less attenuated by the atmosphere. The radiation makes its way through the water column where it is progressively absorbed by pure water, phytoplankton, and detritus. This light attenuation is calculated as a function of water depth and phytoplankton and detritus concentrations, with their respective light attenuation constants k_W , k_C and k_D , as follows:

$$I(z) = I_0 \exp\left(-k_W z - k_C \int_z^\eta P dz - k_D \int_z^\eta D dz\right) \quad (15)$$

In the water column, phytoplankton can utilize this energy for photosynthesis. Nevertheless the amount of PAR that is effectively absorbed by phytoplankton, $f_3(I)$, depends on the intensity of the radiation since effects such as light inhibition take place. It is parameterized using the formulation of Platt et al. (1980):

$$f_3(I) = \left(1 - e^{-\alpha I/\mu_{max}}\right) e^{-\beta I/\mu_{max}} \quad (16)$$


where α and β are the light-photosynthesis slope and the inhibition coefficient. The maximum efficiency is attained at 79 W/m^2 when the intensity is high enough to provide significant energy to phytoplankton but small enough to avoid damaging vegetation tissues. Finally, the effect of phytoplankton on zooplankton grazing is finally parameterized by a Hill–Langmuir equation with a Hill coefficient of 2 and the half-saturation constant K_P .

$$f_4(P) = \frac{P^2}{P^2 + K_P^2} \quad (17)$$


All the ecosystem model parameters are summarized in Table 1. For lack of field data, they could neither be measured directly, nor estimated by inverse modeling from observations of the N , P , Z and D concentrations. We have therefore used the same parameters values as those used by Tian et al. (2015) for a similar modeling study but in a different location. The ecosystem model equations are solved on the same unstructured mesh as the hydrodynamic model equations by using also the DG finite element method.

2.4. Model settings

We simulate the lake dynamics from January 2014 to June 2015, with a time step of 35 s. The model takes about 3 to 4 months to spin up and reach a state in balance with the forcings. As for the spatial discretization, a 2D unstructured mesh is first generated with the open-source mesh generator GMSH (Geuzaine and Remacle, 2009). The mesh resolution depends on the distance to the coast with a maximum mesh resolution of 300 m along the coast of Lago Menor and 800 m along the coast of Lago Mayor. Faraway from the coast, the mesh coarsens and reaches a minimum resolution of 15 km. This allows us to concentrate the computational resources where they are most needed. In particular, the resolution is sufficient to represent the narrow passage of Tiquina connecting both basins. Once the horizontal mesh has been built, the 3D mesh is obtained by extruding it vertically over a maximum of 15 horizontal layers (called z -levels) depending on the water depth. The vertical resolution reaches 1 m in the top layers, where the biophysical processes of interest take place, and coarsens to 60 m in the deepest parts of the lake. In the end, the 3D mesh is composed of a total of 2.1×10^5 triangular prismatic elements (Fig. 4).

The main forcings that drive the water movements in our model are the lake-surface heat and momentum fluxes. The wind data used for this purpose are that of the Climate Forecast System (CFS) provided by the National Oceanic and Atmospheric Administration (NOAA). This reanalysis product provides hourly time series of the u and v components of wind at 10 m over land with a horizontal resolution down to 0.5° . Surface temperature is extracted from the ERA5 climate reanalysis dataset provided by the Copernicus Climate Change Service (C3S). This dataset consists of hourly skin temperature with a spatial resolution of 0.25° . ERA5 provides water surface temperatures as it takes into account water bodies when computing global skin temperatures. Initial water temperatures are set from 12.7° C at the surface to 12° C in the depth, corresponding to typical values for January and initial water velocities and elevations are set to zero.

For lack of more precise field data, the ecosystem model is initialized with spatially homogeneous values for N , P , Z and D throughout the lake. For the nutrients, we use the average nitrogen content ($\text{NO}_2 + \text{NO}_3$) of 1.79 mmol N/m^3 measured by Cruz et al. (2014). Since we did not have field measurements for the other variables, we used the initial values of Tian et al. (2015) and adjusted them so that the ratio with the nutrient concentration is the same in both systems. This leads to initial values of P , Z and D equal to 0.45 , 0.22 and 0 mmol N/m^3 , respectively. Although these initial values are certainly a crude estimate of the real state of the system at the start of the simulation, it is worth noting that the NPZD model sensitivity to the initial conditions is rather weak. After an initial spin-up period of about 3–4 months, the model reaches a state in balance with the forcings and hence “forgets” the initial condition. Furthermore, the coupling between both models being only one-way (from the hydrodynamic model to the NPZD model), any errors in the NPZD model would not impact the hydrodynamic model results.

As shown by the governing equations, the NPZD ecosystem model is driven by physical factors such as water currents or light intensity. In our study, we also pay particular attention to the nitrogen river flux in Lago Menor. However, little data is available to build an accurate forcing. Nutrients provided by the Katari River during 2014 and 2015 are estimated by analyzing the river flow rate provided by the Bolivian Ministry of Environment and Water (MMaYA, 2019) and the concentrations of contaminants provided by different studies (see Appendix A for details). Since the annual flow rates were similar during years 2010 to 2015, we consider the NO_3 concentrations measured during this period as a proxy to reconstruct the monthly values for the year 2014. For instance, measures taken on November 2013 are used to derive NO_3 concentrations in November 2014. This way, we are able to create an approximation of the anthropogenic contamination in NO_3 during 2014 and 2015 (Fig. 5).

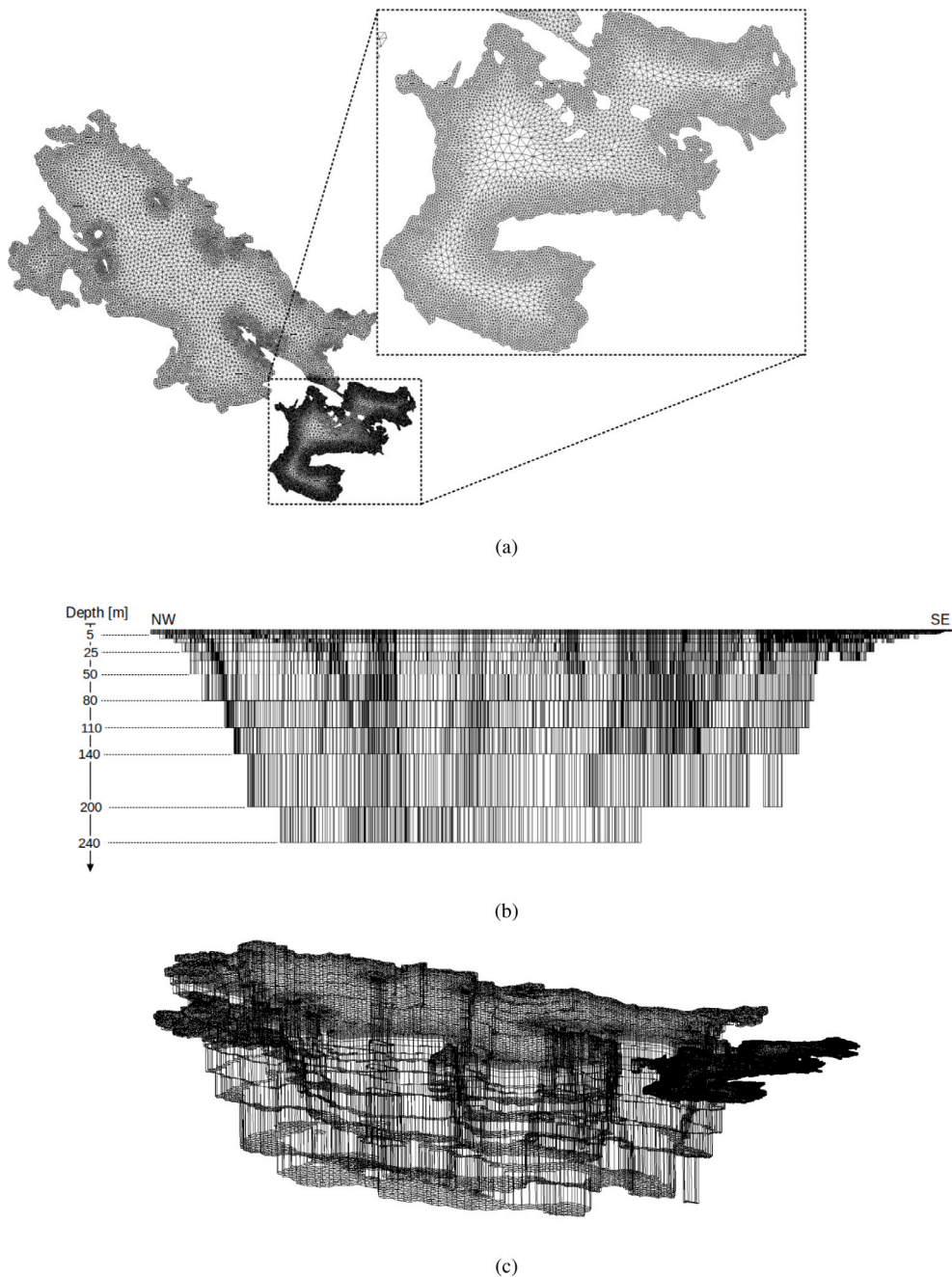


Fig. 4. (a) The horizontal mesh is composed of 2.8×10^4 triangular elements; (b) over the vertical, the horizontal triangular mesh is extruded into up to 15 layers of prisms; (c) the 3D mesh is composed of 2.1×10^5 triangular prismatic elements. Note that scales differ between horizontal and vertical dimensions.

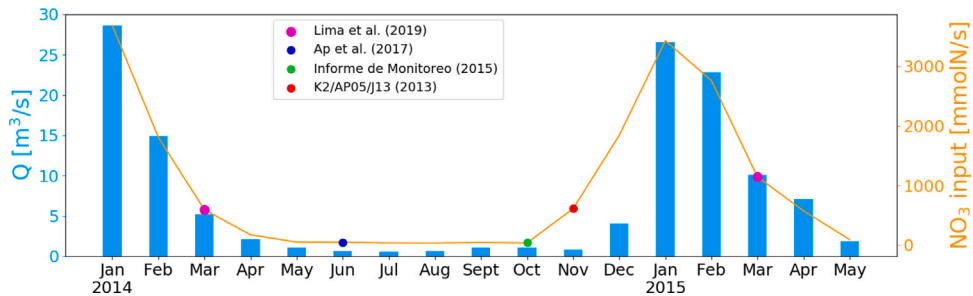


Fig. 5. Discharge and estimated nitrate input from the Katari River.

Table 1
Summary of the parameter values used in the NPZD ecosystem model.

Symbol	Definition	Value	Unit
a	Temperature coefficient	0.07	(°C) ⁻¹
g_{max}	Maximum grazing rate	8.10×10^{-6}	s ⁻¹
I_0	PAR at the surface	275	W/m ²
k_C	Light attenuation by phytoplankton	0.06	m ² (mmol N) ⁻¹
k_D	Light attenuation by detritus	0.01	m ² (mmol N) ⁻¹
k_W	Light attenuation by pure water	0.08	m ⁻¹
K_N	Half-saturation constant for nitrogen uptake	0.50	mmol N m ⁻³
K_P	Half-saturation constant for grazing	0.25	mmol N m ⁻³
m_p	Phytoplankton mortality	9.26×10^{-7}	s ⁻¹ (mmol N m ⁻³) ⁻¹
m_z	Zooplankton mortality	6.94×10^{-7}	s ⁻¹ (mmol N m ⁻³) ⁻¹
s_D	Detritus sinking speed	1.157×10^{-4}	m s ⁻¹
T_{opt}	Optimal temperature	20	°C
μ_{max}	Phytoplankton maximum growth rate	3.25×10^{-5}	s ⁻¹
α	Light-photosynthesis slope	1.62×10^{-6}	m ² s ⁻¹ W ⁻¹
β	Light inhibition coefficient	3.24×10^{-8}	m ² s ⁻¹ W ⁻¹
ϵ	Remineralization rate at 0 °C	1.73×10^{-7}	s ⁻¹
λ	Active respiration	0.30	
γ	Zooplankton growth efficiency	0.40	

Additionally, since the nitrogen-based nutrients in the model also take into account NO₂ concentrations, these are added to the N input forcing following the same NO₃/NO₂ ratio found in Lago Menor: for each mmol N/L of NO₂ we observed 12 mmol N/L of NO₃ as a global mean (Cruz et al., 2014). The total nitrogen input are thus computed as follows:

$$\begin{aligned}
 N_{input} &= [NO_3] + [NO_2] \\
 &= [NO_3] + \frac{1}{12} * [NO_3] \\
 &= \frac{13}{12} * [NO_3]
 \end{aligned} \quad (18)$$

No quantitative data is available concerning ammonium or phosphorus in the lake. Nevertheless, the concentrations of soluble reactive phosphorus (SRP) available for phytoplankton growth are often high in Lake Titicaca relative to the amounts of dissolved inorganic nitrogen (DIN = NO₃⁻ + NO₂⁻ + NH₄⁺). The DIN to SRP ratio, an indication of algal nutrient deficiency, is usually well below 10:1 (Iltis et al., 1992). Phosphorus can thus be neglected in our study since it is not considered as a limiting element.

3. Results

Our model provides the space–time evolution of the water velocity, the temperature and the NPZD components. The results shown here are chosen in order to provide means of determining whether the model is able to accurately simulate the annual physical evolution of the lake. We also study the bloom event simulated in March 2015.

3.1. Water current and temperature

Water currents are mainly influenced by the wind, which blows towards the Southwest through most of the year. As a result, surface waters tend to flow towards the South of the lake (see Fig. 6 showing the yearly average of the surface velocity). There is a global southward surface flow with a maximum velocity of about 5 cm/s in the center of Lago Mayor. On the other hand, Lago Menor shows less pronounced currents due to its shallow nature. In the Cohana Bay, where the N input occurs, currents are quite slow (< 2 cm/s).

The Strait of Tiquina connects both parts of the lake. Although the flow in the passage frequently reverses, there is a net average flow directed towards Lago Menor (not shown). The mean transport ranges from 0.01 to 0.03 m²/s, which leads to yearly volumes of 1 to 10 × 10⁸ m³ flowing through the strait. The discharge barely exceeds 300 m³/s, although our model predicts instantaneous peaks of more

than 1000 m³/s. This flux is one order of magnitude larger than the outflow through the Desaguadero River or the inflow from the Katari River. This supports our hypothesis that the lake is a closed system with regard to water input/output. It also highlights the importance of modeling the circulation in the entire lake and not just in Lago Menor.

The evolution of water temperature within the lake is strongly dependent on the surface temperature. During the cooler dry season, the surface temperature drops from around 15 °C in February to 12.5 °C in July. The surface temperature thus falls to values similar to the temperature in the bottom of the lake (12 °C). The thermocline, a physical barrier separating the warmer surface waters from the underlying cooler waters, is thus much less pronounced than during the wet season. This weakening of the thermocline barrier leads to more vertical mixing between water layers. However, the water column is partially mixed as only the top portion of the water column is affected (Richerson, 1992).

Our model is able to qualitatively reproduce the evolution from a strongly-stratified temperature profile in the summer to an almost vertically-uniform profile in the winter (Fig. 7 for year 2014). In August 2014, it is interesting to note that there is only a 0.5 °C difference between the surface and the lake bottom temperatures. This is enough to restrict the vertical mixing to the top 100 m below the surface. However, in some years, a complete temperature inversion can occur in which the deep waters are warmer than the surface waters. This would result in a complete vertical mixing and occurrences of this phenomenon were recorded in the past (Richerson, 1992).

A more quantitative validation can be achieved by comparing our simulated temperature profiles with the data gathered during the CR-1407 scientific cruise that took place in July 2014 (Cruz et al., 2014). Fig. 8 shows four temperature profiles on different locations around Lake Titicaca. The root mean square error (RMSE) is calculated between the outputs and the observations for each of the 27 profiles in order to evaluate the precision of the model. The results are listed in Appendix B. The simulated results are close to the observations in most cases. However, the model shows non-negligible errors in Lago Menor. This is partially due to the surface boundary condition. Indeed, due to the poor spatial resolution of the skin temperature data, surface temperatures in the Lago Menor and near the edges of the lake were partially affected by the adjacent land surface temperatures during interpolation. Our model performs well at reproducing the temperature evolution towards the depth of the lake with a global mean error of 0.42 °C.

The summer and winter dynamics can be further compared by looking at the temperature spatial variations along a section of the lake for the months of August and December (Fig. 9a). During the wet season (December), Lake Titicaca presents a stratified distribution of water

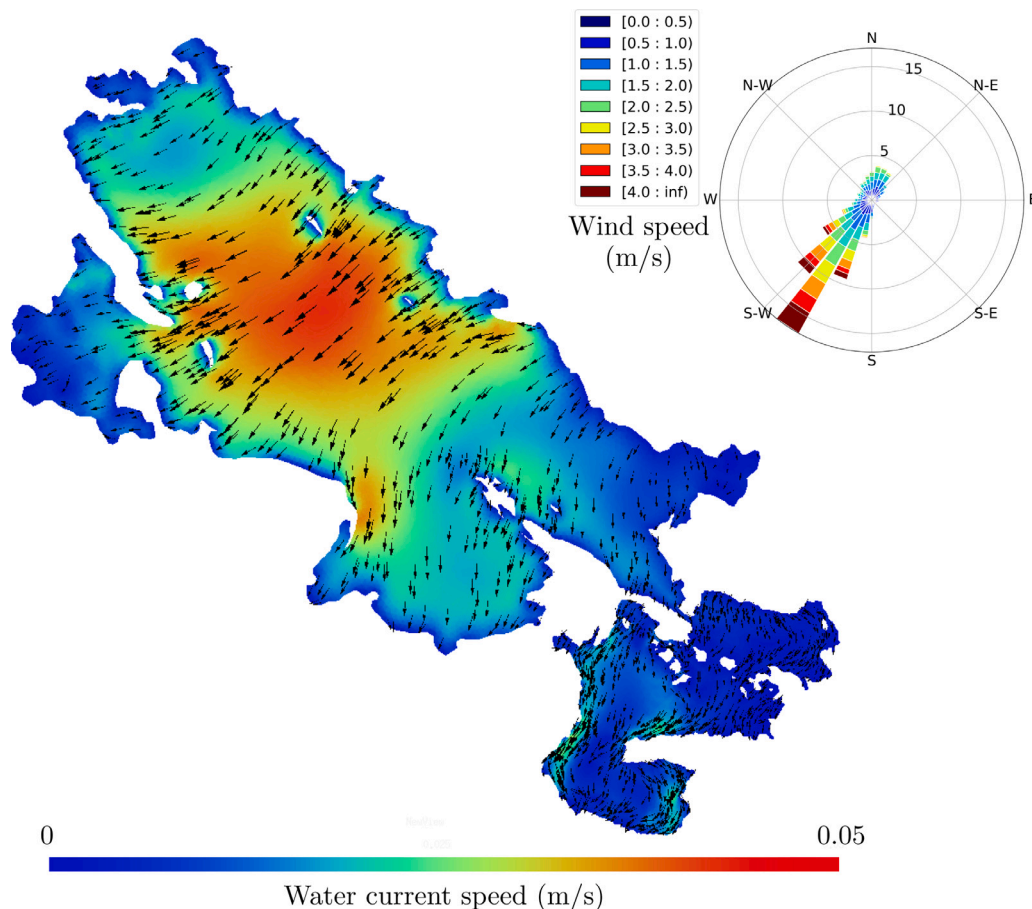


Fig. 6. Yearly average of the surface water horizontal velocities (m/s) in Lake Titicaca during year 2014. The wind-rose shows average wind directions during the year. The average surface flow is mostly directed to the south-west.

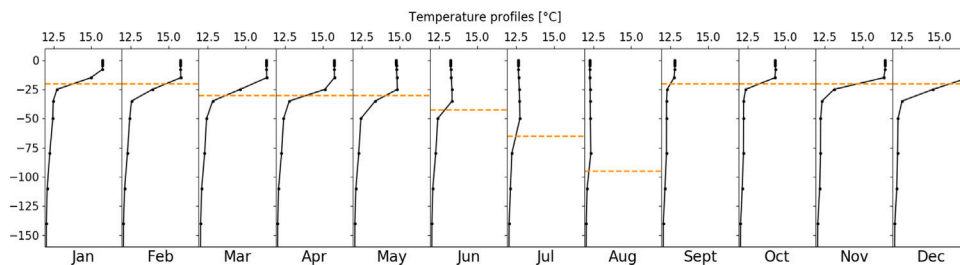


Fig. 7. Evolution of the simulated temperature profile throughout year 2014 in the center of Lago Mayor (lat:-15.66° lon:-69.45°). The temperature (°C) is shown in relation to depth (m) for each month. The horizontal line represents the depth where the biggest temperature gap occurs, therefore symbolizing the approximate depth of the thermocline.

temperature with 17 °C on the surface and 12 °C on the bottom of the lake (see Fig. 9a). The modeled thermocline is located between 20 and 30 m depth. During the cooler dry season, the surface temperature falls to values around 12.5 °C. The temperature gap between the surface and the bottom of the lake is much less pronounced than during the wet season. The clear thermocline thus disappears and is replaced by a smoother thermal gradient. The disappearance of the thermocline can be explained by the effect of the thermal inertia of the lake. Indeed, this inertia is responsible for the slow cooling of waters therefore maintaining warmer temperatures at medium depths than near the surface. This inversion of temperature is what drives the vertical movement of water since the warmer and less dense waters tend to rise.

3.2. NPZD components

The distribution of the NPZD components within Lago Mayor is not directly influenced by river inputs since the influx of *N* is restricted

to Lago Menor. Also, the model sensitivity to the initial conditions is weak. Indeed, several simulations launched with different starting values for the NPZD components take only a few days to reach a similar equilibrium state.

Nutrients are mainly found in the depths of the lake (Fig. 9b). Sinking detritus are also found in these areas (see Fig. 9e), and are the most important source of *N* through the remineralization process. During periods of strong stratification, phytoplankton thrives within a horizontal layer between 25 m and 80 m depth as it requires both nutrients, available below, and sunlight from above (see Fig. 9c and Fig. 9d). Likewise, it is common to find zooplankton in this same thriving region since it solely feeds on phytoplankton through grazing.

Higher phytoplankton concentrations can be found near the edges of the lake. This phenomenon is due to the nitrogen and detritus distributions. Indeed, in these areas, the lake is rather shallow and detritus, which accumulate near the bottom, are closer to the surface. The remineralization process is thus particularly efficient with

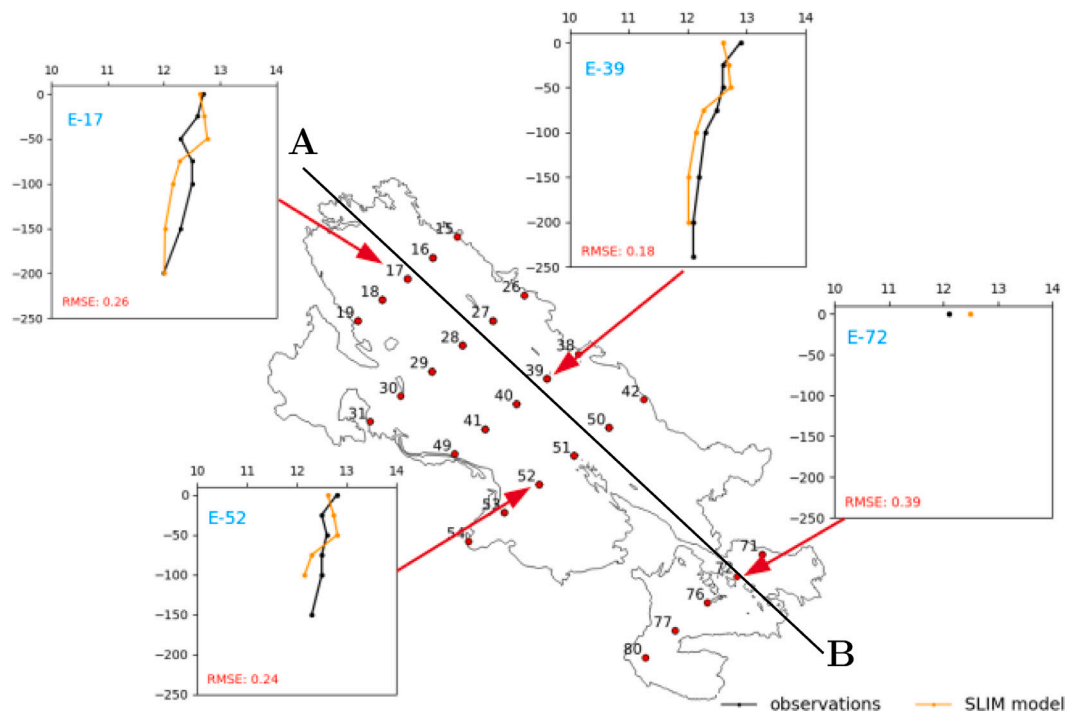


Fig. 8. Temperature profiles comparing simulated outputs with observations from the July 2014 scientific cruise CR-1407 (Cruz et al., 2014). The AB-line represents the cross section in Fig. 9.

the higher temperatures from the proximity with the surface. The high availability of nitrogen in these regions promotes phytoplankton growth. Our results also indicate that phytoplankton, and thus zooplankton, concentrations are generally higher in Lago Menor than in Lago Mayor. These results agree with observations made by Ittis (1992) who mentions that biomass levels during 1985–1987 were 5 to 36 times higher in Lago Menor than in Lago Mayor.

During periods of strong vertical mixing, both phytoplankton and zooplankton are transported towards the surface. In fact, the phytoplankton concentration greatly increases during this period. Since nitrogen becomes available higher in the water column, the phytoplankton is able to survive closer to the lake surface where more light is available. This leads to an increase of phytoplankton and that in turn accelerates zooplankton growth.

3.3. Phytoplankton bloom of March 2015

During the algal bloom event of March–April 2015, high concentrations of *Carteria* sp. were found in the eastern part of Lago Menor. In Fig. 10, we take a closer look at Lago Menor on the 24th of March 2015. Nutrients concentrations are high in the Cohana Bay where the forcing is applied. This is a shallow region with weak currents and where nutrients therefore tend to accumulate. However, the distribution of *N* in this region is not entirely homogeneous. This is partly due to the current directions that disperse the nutrients and the temporal evolution of the *N* flux from the Katari River. Indeed, the input of nitrogen is weaker during the dry season when the river flow is weaker and the waters are less polluted. Currents eventually manage to bring the nutrient around the peninsula towards the north-eastern part of Lago Menor. The same currents are responsible for the spread of detritus towards the north-eastern side of Lago Menor. Phytoplankton, zooplankton and detritus concentrations are also high in the Cohana Bay. This is primarily due to the high nutrient availability that drives the ecosystem forward. The spread of the phytoplankton towards the North-East follows the same pattern as in the satellite imagery around the same date (Fig. 2). The algae spread within the lake following the water currents towards the North-East and the center of Lago Menor. The satellite imagery did not

cover the western part of the basin. A movie showing the phytoplankton evolution is provided in Online Resource 1.

4. Conclusions

We have developed a multi-scale eco-hydrodynamic model of Lake Titicaca that can represent both the complex interplay between biological and physical processes at stake, and the complex topography of the lake. The former is achieved by coupling a state-of-the-art 3D hydrodynamic model with a NPZD ecosystem model. The resulting model includes all the processes required to simulate the space–time evolution of water quality in the lake. The latter is achieved by using novel numerical methods, based on a Discontinuous Galerkin finite element approximation computed on a multi-scale unstructured mesh, to solve the model equations. It allows us to locally increase the resolution to represent small-scale features, such as the narrow passage between Lago Menor and Lago Mayor, without affecting the overall model performance. The resulting model has been validated with all the available observations.

Our results indicate that the coupled SLIM-NPZD model is able to effectively simulate the biophysical dynamics of the lake. The annual evolution of the thermocline shows a loss of stratification during July–August leading to vertical mixing over the top 100 m layer. This simulation concurs with the observations of Richerson (1992), which serve as a validation for the hydrodynamic component of the coupled model. Similarly, the temperature profiles extracted on July 2014 over the depth of the lake are very close to the ones observed by the scientific cruise CR-1407 (Cruz et al., 2014). This confirms the ability of the model to reproduce the thermal stratification of the lake. The lack of validation data concerning water currents prevents us to draw conclusions regarding the quality of the simulated velocity field. Nevertheless, our results are comparable to the velocity computed by Aguirr Cespedes (2009) in his numerical hydrodynamic model of the lake. Overall, the validations indicates that our model is able to effectively represent the global physical behavior of Lake Titicaca.

The NPZD ecosystem model coupled to the hydrodynamic model manages to simulate the stratification of phytoplankton and zooplankton revealing a horizontal thriving zone between 25 m and 80 m below

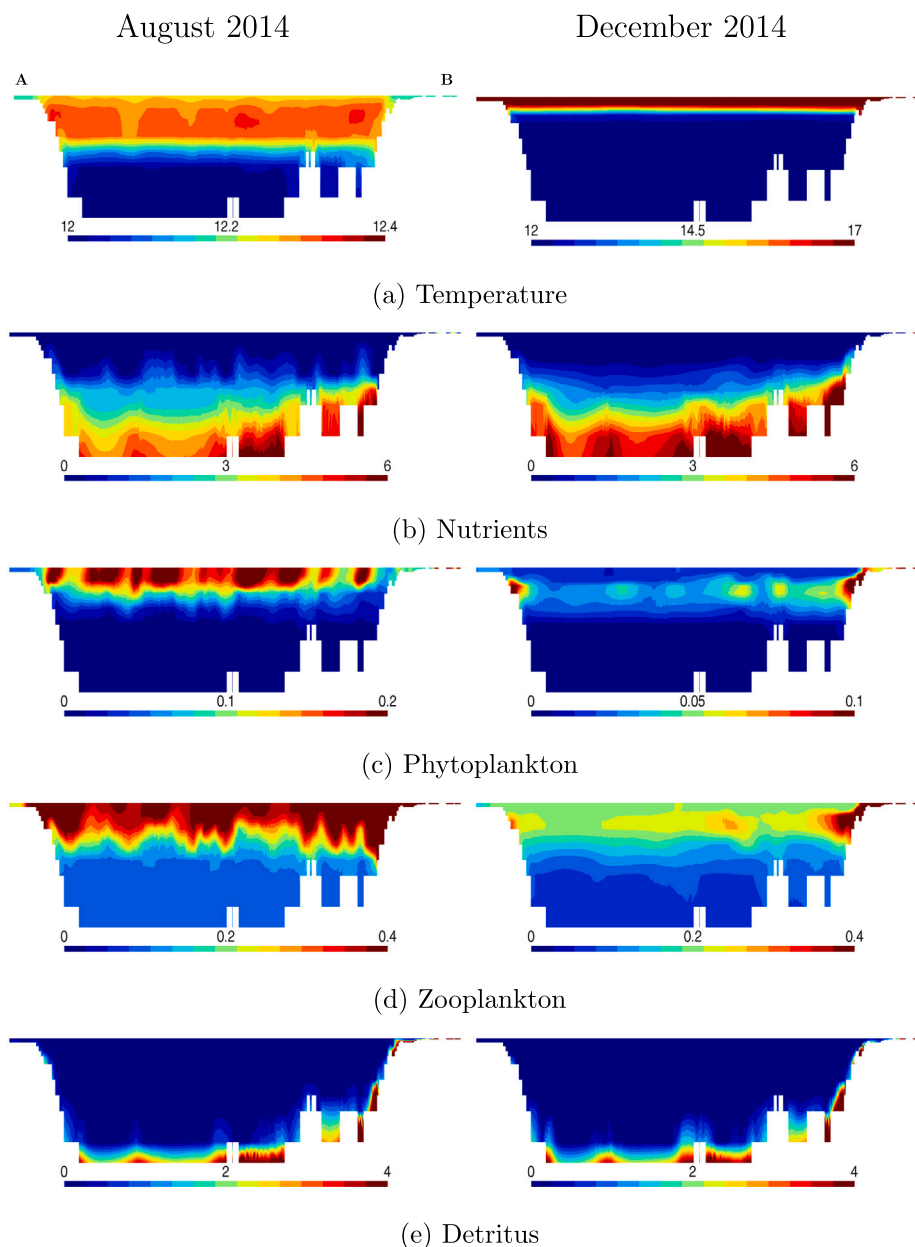


Fig. 9. Temperature ($^{\circ}\text{C}$) and NPZD components (mmol N/m^3) in Lake Titicaca during vertically mixed and stratified conditions in August 2014 (left) and December 2014 (right), respectively. Each cross section spans from the North-West (left) to the South-East (right) of the lake. Note that the colorbar changes between the left and right columns of panels (a) and (c). The cross section is represented by the AB-line in Fig. 8.

the surface during the wet season. Compared to the data presented in Iltis (1992) and Cruz et al. (2014), our model struggles to reproduce the exact vertical distribution of phytoplankton in Lago Menor during the dry season. However, our model manages to correctly simulate the horizontal distribution of phytoplankton within the lake. Indeed, Fig. 10 shows a spread of phytoplankton similar to what occurred during the algal bloom of March–April 2015 (Fig. 2). Likewise, the phytoplankton distribution in Lago Mayor indicates higher concentrations near the edges of the lake, in shallower areas, in agreement with the observations of Iltis (1992).

It is important to mention the structural differences between Lago Mayor and Lago Menor which make them two distinct environments with different hydrodynamics and thus different ecosystemic development schemes. It is thus difficult for a unique model to harness both environments. However, with its variable resolution, SLIM manages to explicitly represent exchanges between both basins through the narrow Strait of Tiquina. This exchange flow largely exceeds rivers

inflow/outflow. The coupled SLIM-NPZD model is thus able to provide realistic simulations of Lake Titicaca as a whole. The model can reproduce the occurrence of vertical mixing during July–August and the related consequences on the NPZD components, as well as the algal bloom event of March–April 2015.

The ability to reproduce these historic conditions given the appropriate input forcing data ensures the validity of the model and enables new research opportunities. Now that the water currents and the dynamics taking place can be simulated, further studies regarding hydrodynamics could be conducted over the entire lake. The spread of contaminants such as mercury, linked to illegal mining activities, or plastic pollution due to uncontrolled urban discharge, can now be simulated and predicted. This would help to better understand the dynamics of the spreads taking place throughout Lake Titicaca. The long-ranging impacts of these pollutions could then be estimated, which could reveal the broader consequences of local contamination sources. Finally, our model would allow to estimate the effect of climate change

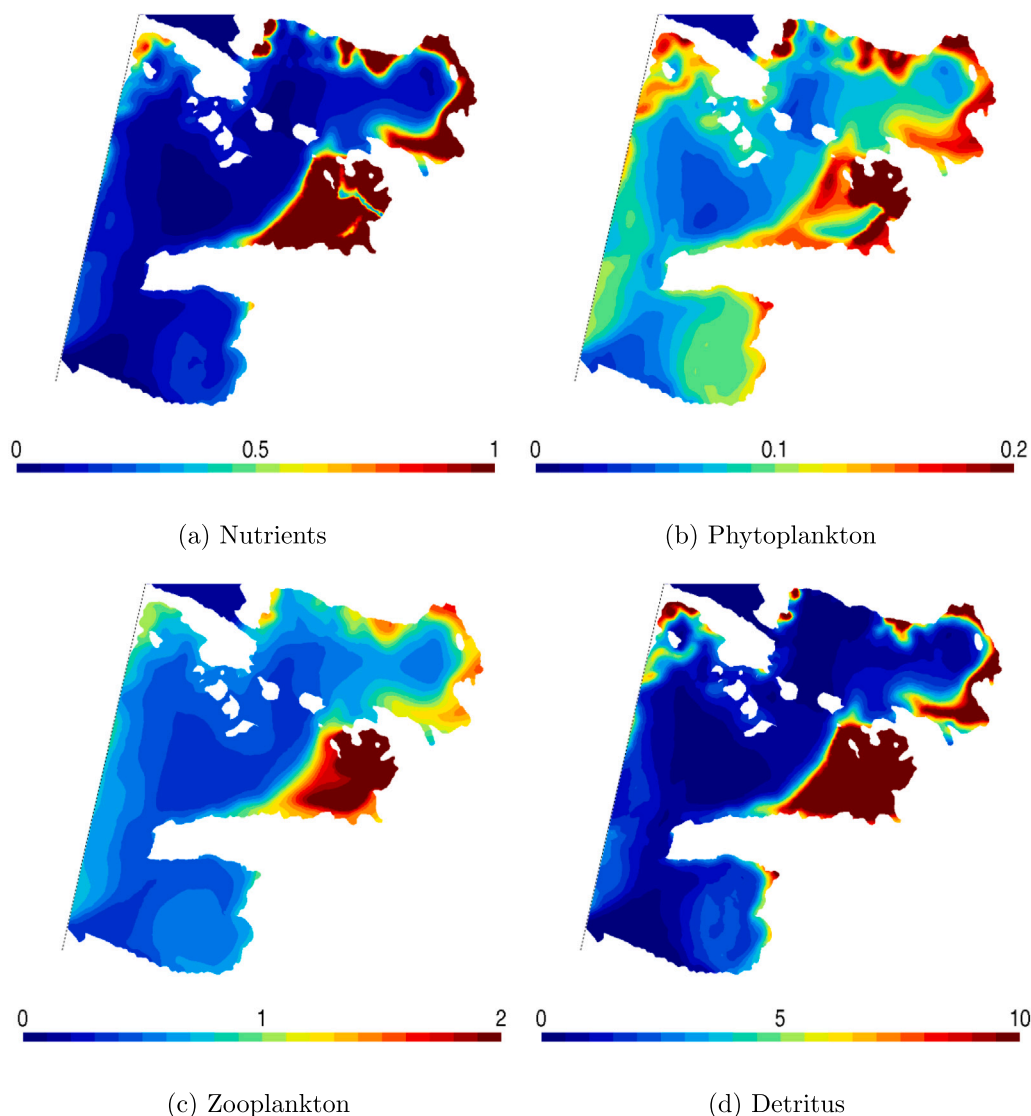


Fig. 10. NPZD components (mmol N/m^3) at the surface of Lago Menor on the 24th of March 2015. Panel (b) is to be compared with Fig. 2.

on the lake ecosystems by, for instance, assessing the impact of rising temperature and decaying nutrients on the phyto- and zooplankton populations.

To better protect the rich biodiversity of the lake and to ensure a durable future for the local populations, environmental policies are being implemented by the Bolivian Ministry of Environment and Water. In this context, our model is a new tool to estimate and predict the impact of human activities on Lake Titicaca's ecosystem. We believe our model could help local authorities to actively manage the lake and the surrounding watershed. For example, to treat the algal bloom events, threshold values of allowed nitrogen discharge could be found which would limit the proliferation of algae. Other uses of the model could be envisioned for other types of pollutions which could help mitigate the negative impacts of human activities on the lake biodiversity.

CRedit authorship contribution statement

François Duquesne: Software, Investigation, Data curation, Writing - original draft, Visualization. **Valentin Vallaeys:** Methodology, Software, Validation, Writing - review & editing. **Prem Jai Vidaurre:** Investigation, Resources. **Emmanuel Hanert:** Conceptualization, Methodology, Validation, Writing - review & editing, Supervision.

Declaration of competing interest

The authors declare that they have no known competing financial interests or personal relationships that could have appeared to influence the work reported in this paper.

Acknowledgments

Computational resources were provided by the Consortium des Équipements de Calcul Intensif (cÉci), funded by the F.R.S.-FNRS under Grant No. 2.5020.11. The authors also wish to acknowledge the Bolivian Ministry of Environment and Water for their help in data gathering.

Appendix A. Nutrient input from the Katari River

Due to the lack of available data concerning the nitrogen discharge of the Katari River, an artificial but realistic forcing is built. This allows us to advance in our research although it is a potential source of error. The N input forcing is computed by considering both the punctual NO_3 concentrations measurements and the 2014–2015 Katari River waterflow. We hypothesize that the NO_3 concentration remains similar each year. For instance, the concentration value in March 2014

Table A.2
Summary of the NO₃ concentration measurements in the Katari river.

NO ₃ (mg/L)	Date of measurement	Analysis method	Detection limit	Source
4.30	June 2012	Ion chromatography Metrohm 732/733 Metrosep A and C2	30–34 µg/L	Ap et al. (2017)
45.65	November 2013	N/A	N/A	K2AP05J13 (2013)
2.04	October 2014	UV–Vis spectroscopy	N/A	MMAyA (2014)
7.00	March 2015	Ion chromatography Dionex ICS 1100	N/A	Lima et al. (2019)

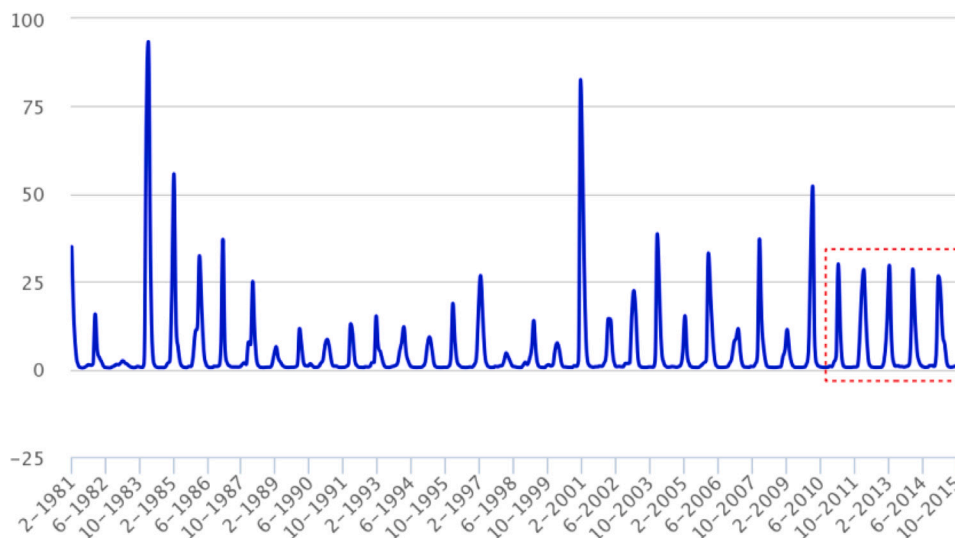


Fig. A.11. Historical values of the Katari River outflow (in m³/s) in Lago Menor. The timeseries shows that there is very little interannual variability during years 2011–2015 (red box).

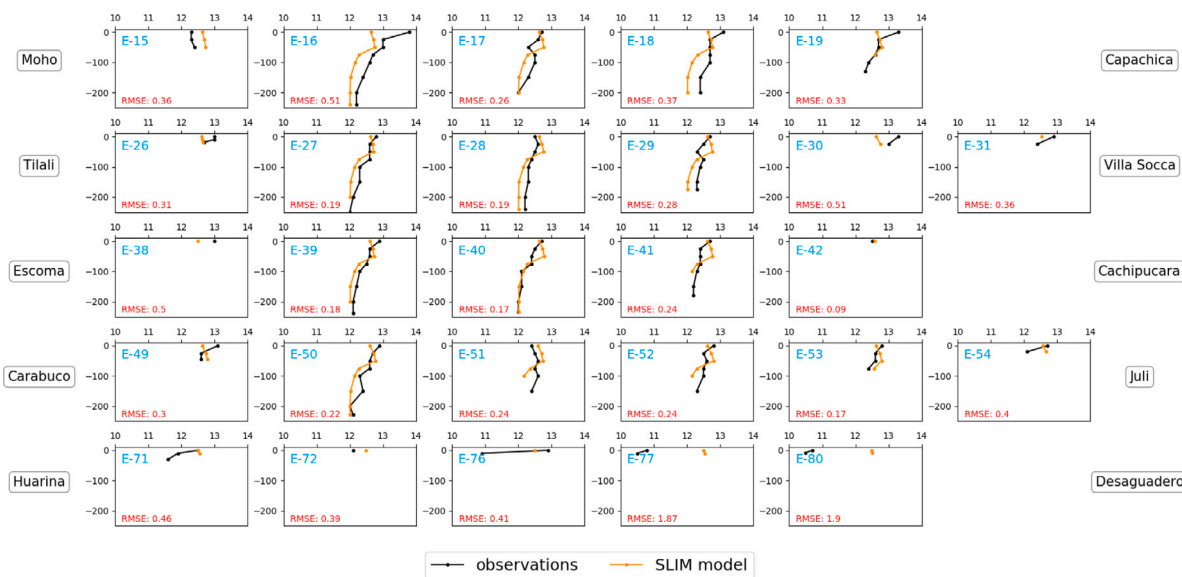


Fig. B.12. Temperature (°C) profiles at the 27 measurement locations. The vertical axis is the depth in meters.

is reported in March 2015. By combining the concentrations with the water flow, we find the amount of NO₃ discharged per second for each month. In a similar way, for the remaining months of the year, data is extrapolated by using plausible concentration values. Waters are less polluted in the dry season since the delta filters out a large amounts of nitrogen. Certain difficulties still remain such as the estimation of the nitrogen provided by the local populations of the Cohana Bay or the amount leached by the neighboring livestock farming activities. Table A.2 shows NO₃ values provided by different sources on different

dates of measurements. Fig. A.11 shows the outflow history of the Katari watershed. The flow rate has the same aspect during the period of 2011 to 2015, with a peak flow at around 30 m³/s. The figure is reproduced from the Geovisor VIBH of the MMAyA (MMAyA, 2019).

Appendix B. Temperature validation plots

Temperature profiles are displayed at 27 measurement locations over Lake Titicaca in Fig. B.12 (Cruz et al., 2014). The root mean square

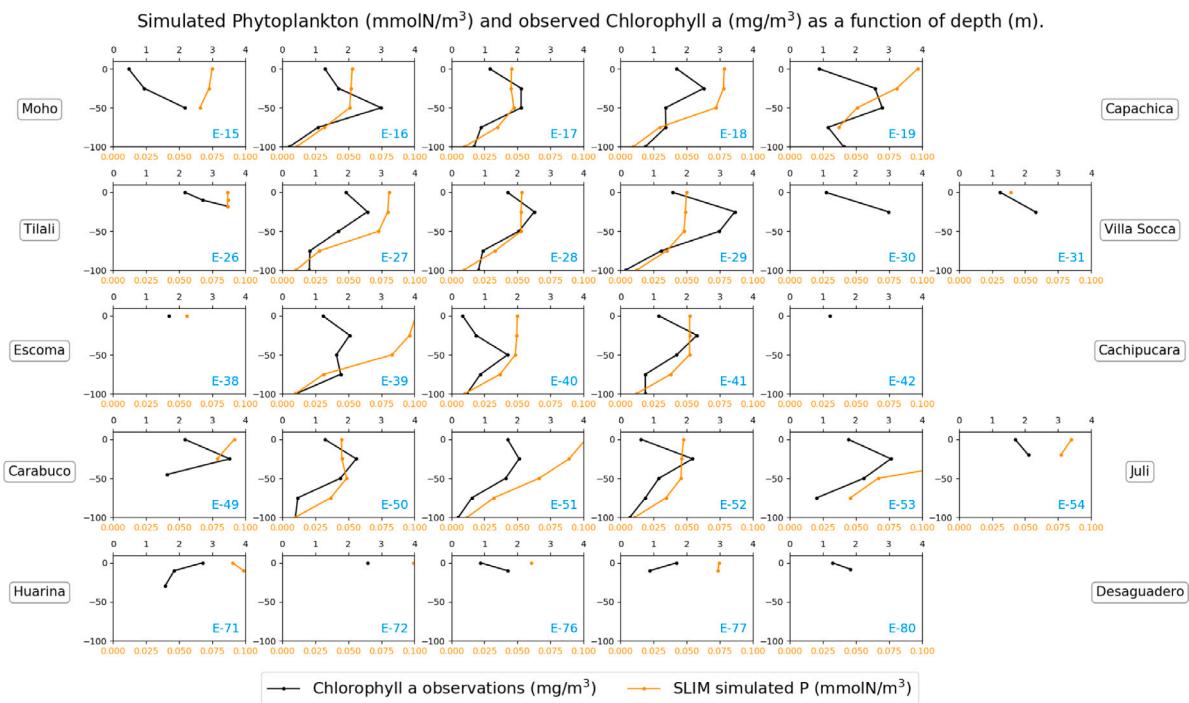


Fig. C.13. Observed Chlorophyll a (mg/m³) and simulated phytoplankton (mmol N/m³) as a function of depth (m).

error (RMSE) is computed for each point by comparing observations with the corresponding simulated values at depths where observations are available.

Appendix C. Validation of the vertical distribution of phytoplankton

Fig. C.13 shows the vertical distribution of simulated phytoplankton (SLIM model) and chlorophyll a concentrations gathered by the Cruz et al. (2014) scientific cruise. The phytoplankton qualitatively represents the observed shape of the chlorophyll a distributions, although detritus also contains part of this chlorophyll a.

Appendix D. Supplementary data

Supplementary material related to this article can be found online at <https://doi.org/10.1016/j.ecolmodel.2020.109418>.

References

Acha, D., Guedron, S., Amouroux, D., Point, D., Lazzaro, X., Fernandez, P.E., Sarret, G., 2018. Algal bloom exacerbates hydrogen sulfide and methylmercury contamination in the emblematic high-altitude Lake Titicaca. *Geosciences* 8 (438).
 Aguirr Cespedes, C.A., 2009. Simulacion numerica de la hidrodinamica del Lago Titicaca, frente a las costas de la ciudad de puno en el Peru. (Master's thesis). Universidad Nacional Mayor de San Marcos, Lima, Peru.
 Ap, D., Duwig, C., Spadini, L., Uzu, G., Guedron, S., C. Morel, M., Cortez, R., Ramo. Ramos, O., Chincheros, J., Martins, J., 2017. How uncontrolled urban expansion increases the contamination of the Titicaca Lake Basin (El Alto La Paz Bolivia). *Water Air Soil Pollut.* 228, <http://dx.doi.org/10.1007/s11270-016-3217-0>.
 Archundia, D., Duwig, C., Lehembre, F., Chiron, S., Morel, M.C., Prado, B., Bourdat-Deschamps, M., Vince, E., Aviles, G.F., Martins, J.M.F., 2017. Antibiotic pollution in the Katari subcatchment of the Titicaca Lake: Major transformation products and occurrence of resistance genes. *Sci. Total Environ.* 576, 671–682. <http://dx.doi.org/10.1016/j.scitotenv.2016.10.129>.
 Bienfang, P., Harrison, P., 1984. Sinking-rate response of natural assemblages of temperate and subtropical phytoplankton to nutrient depletion. *Mar. Biol.* 83, 293–300.
 Cruz, R.C., Cruz, L.L., Calderon, J., Puntaca, L., Casa, C., Yujra, E., Amaru, G., Mamani, H.S., 2014. Crucero de evaluacion de recursos pesqueros y condiciones limnologicas del Lago Titicaca - cr. 1407, <http://dx.doi.org/10.13140/rg.2.1.3385.6084>.

Delandmeter, P., Lambrechts, J., Legat, V., Vallaey, V., Naithani, J., Thiery, W., Remacle, J.F., Deleersnijder, E., 2018. A fully consistent and conservative vertically adaptive coordinate system for SLIM 3D v0.4 with an application to the thermocline oscillations of Lake Tanganyika. *Geosci. Model Dev.* 11, 1161–1179. <http://dx.doi.org/10.5194/gmd-11-1161-2018>.
 Delandmeter, P., Lewis, S.E., Lambrechts, J., Deleersnijder, E., Legat, V., Wolanski, E., 2015. The transport and fate of riverine fine sediment exported to a semi-open system. *Estuar. Coast. Shelf Sci.* 167, 336–346. <http://dx.doi.org/10.1016/j.ecss.2015.10.011>.
 Duwig, C., Archundia, D., Lehembre, F., Spadini, L., Morel, M.C., Uzu, G., Chincheros, J., Cortez, R., Martins, J.M.F., 2014. Impacts of anthropogenic activities on the contamination of a sub watershed of Lake Titicaca. Are antibiotics a concern in the Bolivian altiplano?. *Proc. Earth Planet. Sci.* 10, 370–375. <http://dx.doi.org/10.1016/j.proeps.2014.08.062>.
 Gammons, C.H., Slotton, D.G., Gerbrandt, B., Weight, W., Young, C.A., McNearney, R.L., Camac, E., Calderon, R., Tapia, H., 2006. Mercury concentrations of fish, river water, and sediment in the Rio Ramis-Lake Titicaca watershed, Peru. *Sci. Total Environ.* 368, 637–648. <http://dx.doi.org/10.1016/j.scitotenv.2005.09.076>.
 Geuzaine, C., Remacle, J.F., 2009. Gmsh: A 3-D finite element mesh generator with built-in pre-and post-processing facilities. *Internat. J. Numer. Methods Engrg.* 79, 1309–1331.
 Guedron, S., Point, D., Acha, C., D. Bouchet, S., Baya, P., Tessier, E., Monperrus, M., Molina, C., Groleau, A., Chauvaud, L., Thebault, J., Amice, E., Alanoca, L., Duwig, C., Uzu, G., Lazarro, X., Bertrand, A., Bertrand, S., Barbraud, C., Amouroux, D., 2017. Mercury contamination level and speciation inventory in Lakes Titicaca & Uru-Uru (Bolivia): Current status and future trends. *Environ. Pollut.* 231, 262–270. <http://dx.doi.org/10.1016/j.envpol.2017.08.009>.
 Iltis, A., 1992. Phytoplankton : quantitative aspects and population. In: Dejoux, C., Iltis, A. (Eds.), *Lake Titicaca : A Synthesis of Limnological Knowledge. In: Monographiae Biologicae*, vol. 68, Kluwer Academic, Dordrecht, pp. 182–195.
 Iltis, A., Carmouze, J.P., Lemoalle, J., Arze, C., Quintanilla, J., Guyot, J.L., Wasson, J.G., Calle, H., Richerson, P.J., Wurtsbaugh, W.A., Vincent, W.F., Vincent, C.L., Carney, H.J., Tapia, R.A., 1992. Physico-chemistry. In: Dejoux, C., Iltis, A. (Eds.), *Lake Titicaca: A Synthesis of Limnological Knowledge. In: Monographiae Biologicae*, Springer Netherlands, Dordrecht, pp. 89–160. http://dx.doi.org/10.1007/978-94-011-2406-5_5.
 Jackett, D.R., McDougall, T.J., Feistel, R., Wright, D.G., Griffies, S.M., 2006. Algorithms for density, potential temperature, conservative temperature, and the freezing temperature of seawater. *J. Atmos. Ocean. Technol.* 23, 1709–1728. <http://dx.doi.org/10.1175/JTECH1946.1>.
 K2/AP05/J13, 2013. Informe de auditoria sobre el desempeno ambiental respecto a la contaminacion hidrica en la cuenca del rio Katari y la Bahia de Cohana. Informe no publicado. Ministerio de Medio Ambiente y Agua, Ministerio de Minería y Metalurgia, Ministerio de Relaciones Exteriores, Gobierno Autonomo Departamental de La Paz, Gobiernos Autonomos Municipales de El Alto, Viacha, Laja, Pucarani y Puerto Perez, Empresa Publica y Social de Agua y Saneamiento (EPSAS), Empresa

- Municipal de Aseo de El Alto (EMALT) y el Fondo Nacional de Inversion Productiva y Social (FPS), La Paz. p. 268.
- Komarkova, J., Montoya, H., Komárek, J., 2016. Cyanobacterial water bloom of *limnospira robusta* in the Lago Mayor of Lake Titicaca. Can it develop?. *Hydrobiologia* 764, 249–258.
- Lima, I.Q., Munoz, M.O., Ramos, O.E.R., Bhattacharya, P., Choque, R.Q., Aguirre, J.Q., Sracek, O., 2019. Hydrochemical assessment with respect to arsenic and other trace elements in the Lower Katari Basin, Bolivian Altiplano. *Groundw. Sustain. Dev.* 8, 281–293. <http://dx.doi.org/10.1016/j.gsd.2018.11.013>.
- Luo, L., Wang, J., Schwab, D.J., Vanderploeg, H., Leshkevich, G., Bai, X., Hu, H., Wang, D., 2012. Simulating the 1998 spring bloom in lake michigan using a coupled physical-biological model. *J. Geophys. Res.: Oceans* 117, <http://dx.doi.org/10.1029/2012JC008216>.
- Martine Gonzales, I., Zulet Roncal, R., Panchec. Miranda, A., Sanjine Gotilla, J., 2007. Co-operation on the Lake Titicaca. UNESCO-IHP. 118.
- MMAY, 2014. Anexo 2: Tablas de datos. In: Informe de Monitoreo de Calidad Hídrica Cuenca Katari. Ministerio de Medio Ambiente y Agua.
- MMAY, 2019. Balance hídrico de la cuenca del Rio Katari. URL: <http://vibh.mmaya.gob.bo/vibh/database/r/18823932961109045/data>.
- Molina, C., Lazzaro, X., Guedron, S., Acha, C., D., 2017. Contaminación de la Bahía de Cohana, Lago Titicaca (Bolivia) : Desafíos y oportunidades para promover su recuperación. *Ecol. Bolivia* 52, 65–76.
- Monroy, M., Maceda-Veiga, A., de Sostoa, A., 2014. Metal concentration in water, sediment and four fish species from Lake Titicaca reveals a large-scale environmental concern. *Sci. Total Environ.* 487, 233–244. <http://dx.doi.org/10.1016/j.scitotenv.2014.03.134>.
- Naithani, J., Darchambeau, F., Deleersnijder, E., Descy, J.P., Wolanski, E., 2007. Study of the nutrient and plankton dynamics in Lake Tanganyika using a reduced-gravity model. *Ecol. Modell.* 200, 225–233.
- Okubo, A., 1971. Oceanic diffusion diagrams. *Deep-sea Res.* 18, 789–802. [http://dx.doi.org/10.1016/0011-7471\(71\)90046-5](http://dx.doi.org/10.1016/0011-7471(71)90046-5).
- Olascoaga, M.J., Idrisi, N., Romanou, A., 2005. Biophysical isopycnic-coordinate modelling of plankton dynamics in the Arabian Sea. *Ocean Model.* 8, 55–80. <http://dx.doi.org/10.1016/j.ocemod.2003.12.002>.
- Omlin, M., Reichert, P., Forster, R., 2001. Biogeochemical model of Lake Zürich: model equations and results. *Ecol. Modell.* 141, 77–103.
- Platt, T., Gallegos, C., Harrison, W., 1980. Photoinhibition of photosynthesis in natural assemblages of marine phytoplankton. *J. Mar. Res.* 38, 687–701.
- Richerson, P., 1992. The thermal stratification regime in lake titicaca. In: Dejoux, C., Iltis, A. (Eds.), *Lake Titicaca. A Synthesis of Limnological Knowledge*. pp. 120–130.
- Sarret, G., Guedron, S., Acha, D., Bureau, S., Arnaud-Godet, F., Tisserand, D., Goñi-Urriza, C., Duwig, C., Proux, O., et al., 2019. Extreme arsenic bioaccumulation factor variability in Lake Titicaca, Bolivia. *Sci. Rep.* 9, 1–12.
- Sharip, Z., Yanagawa, R., Terasawa, T., 2016. Eco-hydrodynamic modelling of Chini Lake: model description. *Environ. Model. Assess.* 21, 193–210.
- Smagorinsky, J., 1963. General circulation experiments with the primitive equations: I. The basic experiment. *Mon. Weather Rev.* 91, 99–164.
- Tian, R., Chen, C., Qi, J., Ji, R., Beardsley, R.C., Davis, C., 2015. Model study of nutrient and phytoplankton dynamics in the Gulf of Maine: patterns and drivers for seasonal and interannual variability. *ICES J. Mar. Sci.* 72, 388–402. <http://dx.doi.org/10.1093/icesjms/fsu090>.
- Vallaey, V., Karna, T., Delandmeter, P., Lambrechts, J., Baptista, A.M., Deleersnijder, E., Hanert, E., 2018. Discontinuous Galerkin modeling of the Columbia River's coupled estuary-plume dynamics. *Ocean Model.* 124, 111–124. <http://dx.doi.org/10.1016/j.ocemod.2018.02.004>.
- Vallaey, V., Lambrechts, J., Delandmeter, P., Pätsch, J., Spitz, A., Hanert, E., Deleersnijder, E., 2020. Understanding the circulation in the deep, micro-tidal and strongly stratified Congo River ROFI. *Ocean Model.* submitted for publication.
- Widmer, C., Kittel, T., Richerson, P.J., 1975. A survey of the biological limnology of lake titicaca: With 4 figures and 2 tables in the text. *Verh. Internat. Verein Theor. Angew. Limnol.* 19, 1504–1510.
- Wirrmann, D., Rodrigo, L.A., Binford, M.W., Brenner, M., Engstrom, D.R., 1992. Geomorphology and sedimentation. In: *Lake Titicaca*. Springer, pp. 16–39.